

Article

Tunable Near and Mid-Infrared (1.3–5 μm) Picosecond Pulsed Optical Vortex Parametric Oscillator

Mailikeguli Aihemaiti, Dulikun Sulaiman, Dana Jashaner, Yuxia Zhou, Xining Yang, Zhaoxue Li, Bilali Muhutijiang * and Taximaiti Yusufu * 

Xinjiang Key Laboratory for Luminescence Minerals and Optical Functional Materials, School of Physics and Electronic Engineering, Xinjiang Normal University, Urumqi 830054, China; 18935930314@163.com (M.A.); dulikun1@163.com (D.S.); 18297942653@163.com (D.J.); zhou_yx0801@sina.com (Y.Z.); yangxn1984@126.com (X.Y.); zhaoxue_l@163.com (Z.L.)

* Correspondence: bill@xjnu.edu.cn (B.M.); taxmamat_84@sina.com (T.Y.)

Abstract: In this paper, we present a picosecond pulsed, synchronously pumped optical parametric oscillator producing vortex beam output with tunable wavelengths in the near- to mid-infrared range. The system utilizes a Nd:YVO₄ picosecond pulsed solid-state laser emitting at a wavelength of 1.064 μm to pump a Z-shaped, singly resonant OPO which contains a MgO:PPLN crystal with a fan-shaped grating. The wavelength tuning characteristics of the OPO output are examined both as a function of the MgO:PPLN grating period and crystal temperature. The orbital angular momentum of the pump field can be selectively transferred to either the signal or idler fields by appropriately adjusting the location of the MgO:PPLN crystal within the OPO cavity. The maximum output power of the signal and idler vortex fields are 5.12 W and 3.46 W, respectively, for an incident pump power of 19 W.

Keywords: optical vortex; optical parametric oscillator; nonlinear optics; near- to mid-infrared vortex beam; ultrafast



Citation: Aihemaiti, M.; Sulaiman, D.; Jashaner, D.; Zhou, Y.; Yang, X.; Li, Z.; Muhutijiang, B.; Yusufu, T. Tunable Near and Mid-Infrared (1.3–5 μm) Picosecond Pulsed Optical Vortex Parametric Oscillator. *Photonics* **2024**, *11*, 319. <https://doi.org/10.3390/photonics11040319>

Received: 29 February 2024

Revised: 22 March 2024

Accepted: 27 March 2024

Published: 29 March 2024



Copyright: © 2024 by the authors. Licensee MDPI, Basel, Switzerland. This article is an open access article distributed under the terms and conditions of the Creative Commons Attribution (CC BY) license (<https://creativecommons.org/licenses/by/4.0/>).

1. Introduction

Optical vortex beams possess orbital angular momentum (OAM) and have a helical wavefront and a phase singularity. When theoretically describing these beams, these characteristics manifest in an azimuthal phase term, $e^{il\phi}$, where l represents the OAM [1,2]. Optical vortex beams have found a use in applications including optical communications [3,4], optical trapping [2], ultrafast closed-loop spectroscopy [5,6], quantum optics [7–10], and fine trapping and rotation of particles [11,12]. Optical vortex beams have the capacity to impart momentum to physical media and can twist materials to produce novel micro- and nano-structures which may be useful for new technologies such as chiral-sensitive nano-imaging systems and planar metamaterials [13,14]. While optical vortex beams have enabled a range of new technologies, they are still somewhat limited with respect to their wavelength diversity and OAM control. As such, it is crucial that new techniques are developed which can facilitate such diversity and control, and thus expand the range of applications for these types of beams. Nonlinear frequency conversion techniques including second-harmonic generation [15], sum-frequency generation [16,17], optical parametric oscillation (OPO) [18–22], optical parameter amplification [23], and stimulated Raman scattering [24] are perhaps the most commonly applied laser wavelength conversion techniques. In particular, OPOs are commonly used for the generation of near- to mid-infrared, continuously wavelength-tunable laser emissions with high output power, and work across all temporal modalities (continuous wave to ultrashort pulse). In the context of vortex laser beams, OPOs have been utilized for wide wavelength conversion [25] and OAM transfer (from the pump field to either the signal or idler fields) [26–29].

One of the key applications for vortex laser beams in the near-infrared (1.5–2 μm) wavelength range is optical communications [30,31]. This is due to commercial quartz optical fibers having low loss in this wavelength band, and the OAM characteristics of these beams can be used as an additional degree of freedom for carrying information [32,33]. Vortex beams operating in the mid-infrared region have potential use in applications including quantum optics, materials processing, novel medical diagnosis and treatment, and infrared optoelectronic countermeasures. These applications are made possible due to the characteristic absorption spectra of a wide range of molecules and atoms in the mid-infrared (3–5 μm) wavelength range [34].

The field of ultrafast optics has seen rapid development with the advent of ultrafast lasers which have extremely short pulse durations and ultrahigh peak powers. One of the most interesting aspects of vortex laser research is the application of ultrafast optics with vortex laser beams. This has spawned a wave of new research in topics including nonlinear optics, stimulated emission loss microscopy, and chiral metal nano-structuring [35–37]. In particular, optical vortex beams with a picosecond pulse duration have been used to great effect for the fabrication of high aspect-ratio chiral nano-structures, leveraging the cold ablation effect [38]. We anticipate that picosecond pulsed optical vortex beams with wavelengths in the near- and mid-infrared region will be used as an enabling technology in fields such as molecular spectroscopy and organic materials processing.

Recently, there have been a number of reports demonstrating the operation of a synchronously pumped optical parametric oscillator which generates picosecond optical vortex pulses in the near- and mid-infrared wavelength region by using an X-type cavity [39–42]. The reports highlight the complexity of X-type OPO cavities and their limited wavelength tunability. In these reports, the broadest wavelength tuning range from the OPO was 2538–4035 nm and the maximum output power was 2.2 W. The generation of OPO output wavelengths beyond 4 μm is challenging due to the increasing absorption characteristics of nonlinear crystals (in particular, MgO:PPLN) in the mid- to long-infrared wavelength ranges.

In our prior work, we have reported a synchronously pumped, singly resonant (for the signal field), Z-type OPO with a very high cavity Q-factor [43]. This system produced vortex laser output with tunable output wavelengths in the range of 2.6–5 μm . The maximum vortex output power that could be achieved was 3.7 W, at a wavelength of 2.6 μm , for an incident pump power of 15 W. We note that the very high Q-factor of the singly resonant cavity prohibited oscillation of the signal field beam with a vortex mode and, as such, the OAM of the incident pump beam was always transferred to the idler field.

In this body of work, we investigate the controlled transfer of OAM from the incident pump field to the signal and idler fields by using a Z-shaped, singly resonant (for the signal field), synchronously pumped OPO cavity with a low cavity Q-factor. This OPO can control the transfer of OAM by simply modulating the crystal position. We demonstrate the effective generation of near- and mid-infrared picosecond pulsed vortex outputs with wavelength tuning across the range of 1.3–5 μm by changing both the grating period and temperature of the MgO:PPLN crystal. The OAM of the pump beam could be selectively transferred to either the signal or idler fields, adjusting the position of the MgO:PPLN crystal relative to the focusing cavity mirrors. At a maximum incident pump power of 19 W, the output signal vortex field at 1743 nm had a maximum output power of 5.12 W, and the idler vortex field at 2731 nm had a maximum output power of 3.46 W, with conversion efficiencies of 27% and 18.2%, respectively.

2. Experimental Method

The experimental setup of the near- to mid-infrared picosecond pulsed vortex OPO is shown in Figure 1a. An all-solid-state Nd:YVO₄ laser (a pulse width of 15 ps, a repetition rate of 120 MHz, and a maximum output power of 20 W emitting) at 1064 nm with long lifetime, compact structure, high stability, and a Gaussian spatial intensity profile ($M^2 < 1.3$) was used as the pump source. A half-wave plate (HWP) and a polarizing beam splitter

(PBS) were used to control the power of the pump field. A second $\lambda/2$ plate was used to adjust the polarization of the pump beam relative to the crystal axis of the MgO:PPLN, so as to achieve type 0 ($e \rightarrow e+e$) phase-matching of the parametric process. To convert the Gaussian pump beam to a vortex beam, a spiral phase plate (SPP) azimuthally divided into 16 segments was used. The SPP used in the experiment was made of quartz, so it had a high damage threshold and a power loss of 4% to the pump beam. The spatial profile of the generated vortex pump beam is shown inset in Figure 1a, which ensures OPO with vortex beam and extracavity pumping. A lens with a focal length of 125 mm was used to focus the pump vortex beam to a spot with a waist radius of 90 μm at the center of the MgO:PPLN crystal. The MgO:PPLN crystal had a MgO doping of 5% and was 50 mm long, 16 mm wide, and 2 mm thick. The fan-out grating in the MgO:PPLN crystal had a variable period which ranged from 26 to 32 μm . The crystal was mounted in a compact oven which enabled control of the crystal temperature from 25 to 200 $^\circ\text{C}$ with a precision of 0.1 $^\circ\text{C}$. The oven was mounted on a 3-axis translation stage which enabled precise positioning of the MgO:PPLN crystal in both y -axis and x -axis directions, as shown in Figure 1b. By changing the position of the MgO:PPLN crystal on the y -axis, different grating periods could be accessed for wavelength tuning of the signal and idler fields. Horizontal (x -axis) positioning changed the location of the MgO:PPLN crystal relative to the cavity mirrors; as will be detailed further, this influenced the OAM-transfer properties of the system. The two end faces of the MgO:PPLN crystal were coated anti-reflecting for wavelengths of 1.064 μm (pump field), 1.4–1.75 μm (signal field), and 2.5–5 μm (idler field) outputs.

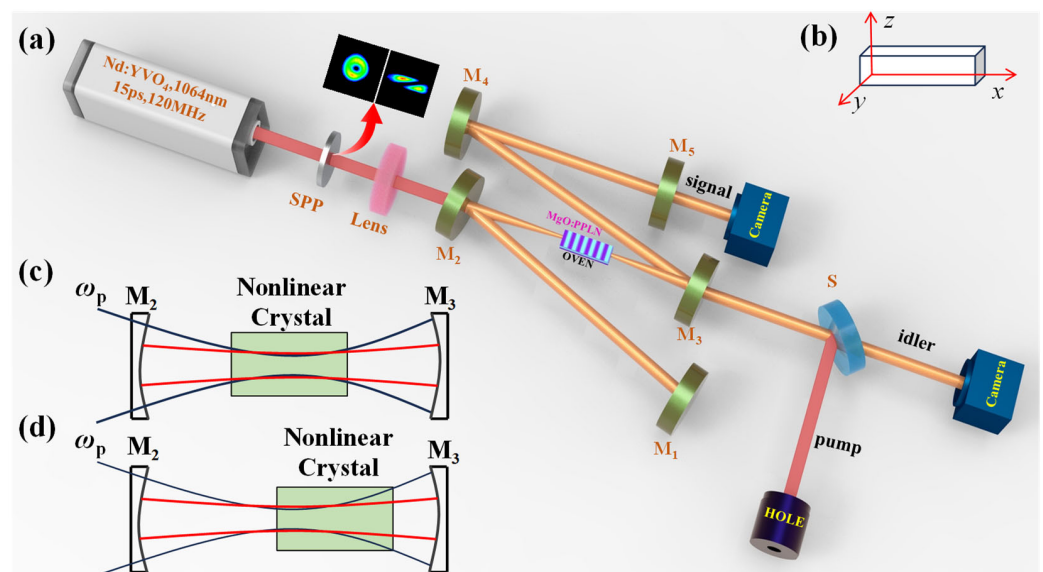


Figure 1. (a) Experimental setup of the picosecond, vortex-pumped OPO. SPP, spiral phase plate; S, wavelength separators; M, mirrors. The inset show the spatial intensity profile of the vortex pump beam in free-space and when focused through a tilted lens (showing the presence of OAM). (b) Schematic diagram of MgO:PPLN at 3-axis translation. (c) Cavity structure in which the nonlinear crystal is located at the confocal center between M2 and M3. (d) Cavity structure in which the position of the crystal is displaced (by 10 mm) from the confocal center between mirrors M2 and M3.

The OPO was designed to be synchronously pumped (with the cavity round-trip time matched with the repetition rate of the pump laser), singly resonant for the signal field, and comprised a standing wave Z-shaped cavity with five mirrors. Plane-concave mirrors M2 ($R = 150$ mm) and M3 ($R = 150$ mm) were positioned 90 mm from the two end faces of the MgO:PPLN crystal. A plane-concave mirror M4 ($R = 500$ mm) and two flat mirrors M1 and M5 were incorporated to form the OPO cavity. Mirrors M1–M4 were coated high-reflecting for the signal field (1.4–1.75 μm , $R > 99.9\%$) and coated anti-reflecting for the pump and idler fields (1064 nm, $R < 0.5\%$; 2.5–5 μm , $R < 2\%$). Mirror M5 was coated

partially transmitting for the signal field (1.4–1.75 μm , $R \sim 80\%$) to ensure the signal field resonated within the cavity (with low Q factor).

In order to examine the mechanism of OAM transfer between the pump and output fields of this OPO, the relative distance between each end of the MgO:PPLN crystal and the cavity focusing mirrors M2 and M3 was varied. This had the effect of changing the spatial overlap between the pump, signal, and idler fields. The total length of the OPO cavity remained unchanged to maintain pump synchronization. The signal and idler fields were extracted from the OPO through mirrors M5 and M3, respectively. The spatial profiles of these fields were imaged using a Spiricon pyroelectric camera III (Ophir-Spiricon, LLC, 3050 North 300 West, North Logan, UT 84341, USA).

3. Experimental Results and Discussion

We observed that the OAM of the pump field could be transferred to either the signal or idler fields depending upon the position of the MgO:PPLN crystal relative to mirrors M2 and M3. To better understand this observation, we undertook a theoretical analysis wherein we calculated the spatial overlap integral η between the interacting fields within the OPO. As outlined in ref. [18], the spatial overlap efficiency is a function of the radii of the pump (ω_p) and resonant signal (ω_s) fields. We theoretically estimated the beam radius of the pump and signal fields at various points within the cavity, between M2 and M3. As shown in Figure 1c,d, the beam radius of the pump beam remains relatively invariant at $\sim 90 \mu\text{m}$ for all positions between M2 and M3 (black lines). This is in contrast to the beam radius of the signal field which has a distinct waist (with minimum radius of $94 \mu\text{m}$) centered between M2 and M3, which diverges significantly towards each of the mirrors. The spatial overlap efficiency between the pump and signal fields at the confocal center between mirrors M2 and M3 was 99.7%. When the MgO:PPLN crystal was positioned in the center, between M2 and M3 (Figure 1c), the high overlap efficiency ensured that the OAM of the pump field was transferred to the signal field. In this case, the idler field was generated with a Gaussian spatial profile. A summary of results is shown in Figure 2.

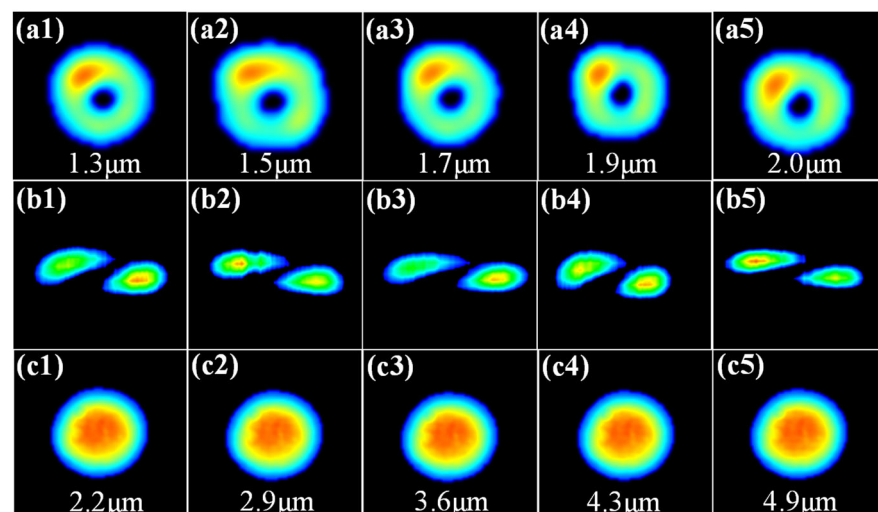


Figure 2. Images showing the spatial intensity profiles of the signal (a1–a5) and idler outputs (c1–c5) from the OPO when the MgO:PPLN crystal was centered between M2 and M3. Images (b1–b5) show the spatial intensity profiles of the signal beam when focused through a tilted lens.

Figure 2(a1–a5) show the spatial intensity profiles of the generated signal field at a range of output wavelengths; in each case, an annular spatial profile with a central null was observed. To determine the order of the vortex signal output, we used the tilted lens method [44]. In this method, when a vortex beam of order l passes through a tilted lens, it is transformed into a multi-lobed beam with $l + 1$ lobes at the focal plane of the lens. Figure 2(b1–b5) show the spatial profile of each of the vortex signal beams when focused

using a tilted lens ($f = 300$ mm); images were taken at the focal plane of the tilted lens. In each case, the focused beams exhibited two lobes confirming that the generated signal beams had an order of 1, which was identical to that of the pump field. Figure 2(c1–c5) show the spatial intensity profiles of the generated idler beams; in each case, they exhibit a near-Gaussian distribution with the beam quality factor (M^2) as 1.3 horizontally and 1.3 vertically, respectively. From the results of Figure 2, it is evident that the OAM of the pump beam is transferred to the signal beam, while the corresponding idler field takes on a Gaussian distribution, thus indicating conservation of OAM in this system.

From our theoretical analysis, we established that the spatial overlap between the pump and signal fields within the MgO:PPLN crystal could be changed simply by adjusting the position of the crystal between mirrors M2 and M3. By moving the position of the crystal 10 mm from the confocal center position between M2 and M3, as shown in Figure 1d, the spatial overlap efficiency between the pump and signal fields was reduced to 80%. We posited that the lower overlap efficiency would limit the ability of the signal field to oscillate as vortex mode, and we expected that the OAM of the pump would be transferred to the nonresonant idler field to fulfil conservation of OAM. This prediction was confirmed in our experiments and the spatial intensity profiles of the generated signal and idler fields are shown in Figure 3. The signal field exhibited a near-Gaussian spatial profile across a range of output wavelengths, as shown in Figure 3(a1–a5). In contrast, the idler field exhibited an annular spatial profile with a central null, as shown in Figure 3(b1–b5); spatial profiles are shown for a range of idler wavelengths. The spatial profiles of the idler field when focused using a tilted lens are shown in Figure 3(c1–c5); these profiles confirm that the idler field had the same OAM as the pump field. It is noteworthy that, when the crystal is at the center of M2 and M3, the signal beam oscillates as vortex mode and the corresponding idler beam generates with Gaussian mode; as the crystal is moved to ~ 5 mm, the signal and idler beams are obtained with mixed mode (incoherent superposition of a fundamental Gaussian mode and a first-order optical vortex mode, caused by nonmonochromaticity from the PPLN crystal); when the crystal is moved to 10 mm from its original center position, the signal beam oscillates as Gaussian mode and the corresponding idler beam generates with vortex mode.

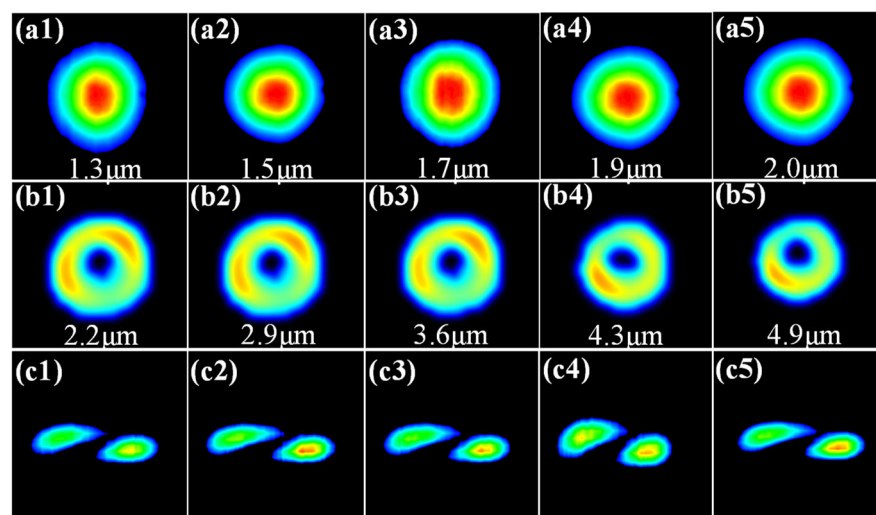


Figure 3. Images showing the spatial intensity profiles of the signal (a1–a5) and idler outputs (b1–b5) from the OPO when the MgO:PPLN crystal was offset by 10 mm from the central position between M2 and M3. Images (c1–c5) show the corresponding spatial intensity profiles of the idler beam when focused through a tilted lens.

We examined the wavelength tunability of the signal and idler fields generated from the OPO, and representative spectra are shown in Figure 4. In the first instance, tunability was examined by way of changing the grating period of the MgO:PPLN crystal and

maintaining a fixed crystal temperature of 25 °C. When the utilized grating period changed from 26 to 32 μm, the wavelength of the signal and idler fields changed from 1354 to 1738 nm and 2743 to 4956 nm, respectively. The tuning ranges of the signal and idler field outputs could be further extended by changing the temperature of the crystal. By increasing the temperature of the crystal to 190 °C, the wavelength of the signal field could be extended to 2015 nm and the wavelength of the idler field shortened to 2254 nm. We also estimated the full width at half maxima (FWHM) of the signal and idler outputs at different wavelengths, and resulting FWHMs of 1.99 nm (1.74 nm), 2.34 nm (2.15 nm), 2.37 nm (2.25 nm), 2.56 nm (2.58 nm), and 2.72 nm (2.70 nm) were obtained at center wavelengths of 1358 nm (4776 nm), 1522 nm (4096 nm), 1683 nm (3687 nm), 1818 nm (2891 nm), and 2018 nm (2253 nm), respectively.

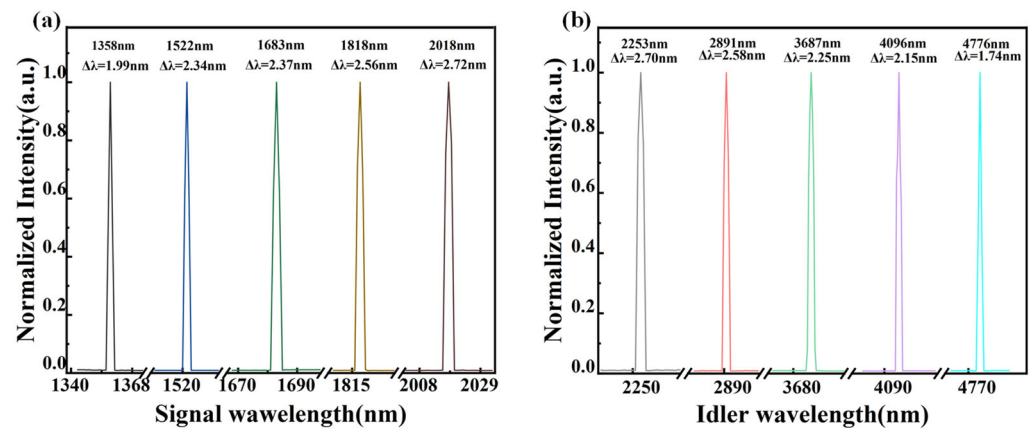


Figure 4. The plots show representative spectral outputs of (a) the signal field and (b) the idler field, as generated from the OPO. The spectra highlight the range of wavelengths that can be generated from the system when changing both the MgO:PPLN grating period and temperature.

We investigated the change in maximum output power of the signal and idler fields generated from the OPO as a function of wavelength and for a fixed incident pump power of 19 W; these plots are shown in Figure 5. When the incident pump power was 19 W, the maximum signal field vortex output power achieved was 5.12 W at 1.74 μm and the maximum idler field vortex output power achieved was 3.46 W at 2.73 μm, with conversion efficiencies of 27% and 18.2%, respectively. As can be seen from the curves, the output power of the signal and the idler fields increases and then decreases as the wavelength increases. There are a number of reasons for this characteristic. These include quantum loss and a reduction in the wavelength conversion efficiency as the difference in wavelength between the pump field and that of the signal and idler fields increases, and an increase in photon absorption within the MgO:PPLN crystal for increasingly longer wavelengths. The cavity mirrors used in this OPO also contribute to this observed characteristic, as they have limited reflectivity outside the range of 1.4–1.75 μm. The high output power and conversion efficiency could be achieved from a fundamental Gaussian beam pumped OPO by a careful design of cavity, which satisfies the good overlap efficiency between the pump and resonant signal beam [45].

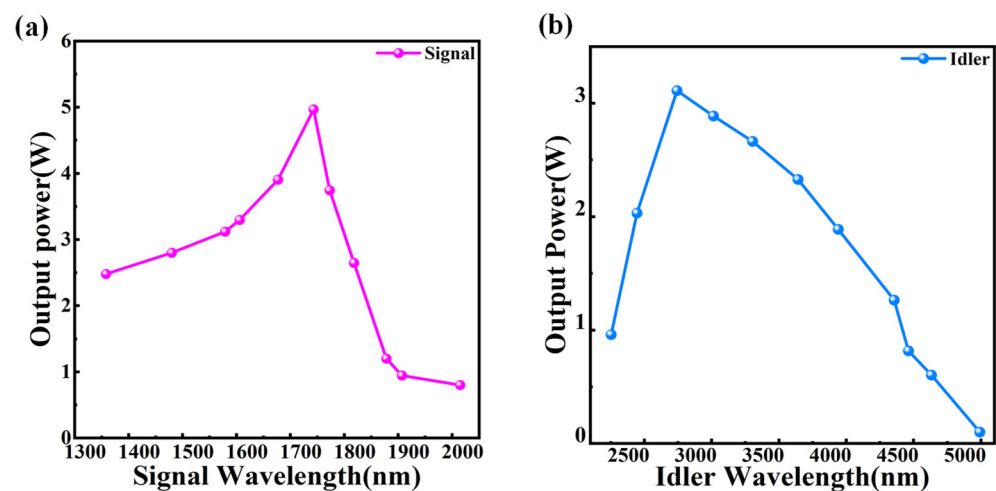


Figure 5. Plots showing (a) the signal field vortex output power and (b) the idler field vortex output power, both as functions of wavelength, with the incident pump field power fixed at 19 W.

4. Conclusions

We have demonstrated the design and operation of a synchronously pumped picosecond pulsed OPO, generating vortex beam output with wavelength tunability in the near- to mid-infrared wavelength range of 1.3–5 μm . Wavelength tunability was achieved by varying both the grating period and temperature of the OPO crystal (MgO:PPLN). The low-Q cavity design of the OPO and precise positioning of the MgO:PPLN crystal enabled preferential transfer of the OAM of the pump field to either the signal or idler fields. At a pump power of 19 W, a maximum signal field vortex output power of 5.12 W was achieved at a wavelength of 1743 nm and a maximum idler field vortex output power of 3.46 W was achieved at a wavelength of 2731 nm. We anticipate that such an OPO design, which is capable of generating multi-Watt vortex output modes with wavelengths in the near- to mid-infrared range, may find significant utility in applications such as optical communications and materials processing.

Author Contributions: Conceptualization, B.M. and T.Y.; methodology, M.A. and B.M.; software, M.A.; validation, B.M., X.Y., T.Y. and D.S.; formal analysis, M.A.; investigation, M.A.; resources, D.J.; data curation, M.A., D.J., Y.Z., B.M. and Z.L.; writing—original draft preparation, M.A., Z.L., B.M., D.S. and T.Y.; writing—review and editing, T.Y. and X.Y.; visualization, M.A.; supervision, T.Y. and B.M.; project administration, T.Y.; funding acquisition, T.Y. All authors have read and agreed to the published version of the manuscript.

Funding: This work was supported by the National Natural Science Foundation of China (Grant No. 12264049, 11664041) and the Foundation of Xinjiang Normal University Young Outstanding Talent Programmer (Grant No. XJNUQB2022-17).

Institutional Review Board Statement: Not applicable.

Informed Consent Statement: Not applicable.

Data Availability Statement: The raw data supporting the conclusions of this article will be made available by the authors on request.

Conflicts of Interest: The authors declare no conflicts of interest.

References

- Allen, L.; Beijersbergen, M.W.; Spreeuw, R.J.C.; Woerdman, J.P. Orbital Angular Momentum of Light and the Transformation of Laguerre-Gaussian Laser Modes. *Phys. Rev. A* **1992**, *45*, 8185–8189. [[CrossRef](#)] [[PubMed](#)]
- Shen, Y.; Wang, X.; Xie, Z.; Min, C.; Fu, X.; Liu, Q.; Gong, M.; Yuan, X. Optical Vortices 30 Years on: OAM Manipulation from Topological Charge to Multiple Singularities. *Light Sci. Appl.* **2019**, *8*, 90. [[CrossRef](#)] [[PubMed](#)]

3. Xia, T.; Xie, Z.; Yuan, X. Multidimensional Multiplexing Holography Based on Optical Orbital Angular Momentum Lattice Multiplexing. *Adv. Photon. Nexus* **2024**, *3*, 016005. [[CrossRef](#)]
4. Reddy, A.N.K.; Anand, V.; Khonina, S.N.; Podlipnov, V.V.; Juodkazis, S. Robust Demultiplexing of Distinct Orbital Angular Momentum Infrared Vortex Beams into Different Spatial Geometry Over a Broad Spectral Range. *IEEE Access* **2021**, *9*, 143341–143348. [[CrossRef](#)]
5. Gao, X.; Zhao, Y.; Wang, J.; Lu, Y.; Zhang, J.; Fan, J.; Hu, M. Spatiotemporal Optical Vortices Generation in the Green and Ultraviolet via Frequency Upconversion [Invited]. *Chin. Opt. Lett.* **2023**, *21*, 080004. [[CrossRef](#)]
6. Ueno, Y.; Toda, Y.; Adachi, S.; Morita, R.; Tawara, T. Coherent Transfer of Orbital Angular Momentum to Excitons by Optical Four-Wave Mixing. *Opt. Express* **2009**, *17*, 20567–20574. [[CrossRef](#)] [[PubMed](#)]
7. Shigematsu, K.; Toda, Y.; Yamane, K.; Morita, R. Orbital Angular Momentum Spectral Dynamics of GaN Excitons Excited by Optical Vortices. *Jpn. J. Appl. Phys.* **2013**, *52*, 08JL08. [[CrossRef](#)]
8. Nagali, E.; Sciarrino, F.; De Martini, F.; Marrucci, L.; Piccirillo, B.; Karimi, E.; Santamato, E. Quantum Information Transfer from Spin to Orbital Angular Momentum of Photons. *Phys. Rev. Lett.* **2009**, *103*, 013601. [[CrossRef](#)]
9. Leach, J.; Padgett, M.J.; Barnett, S.M.; Franke-Arnold, S.; Courtial, J. Measuring the Orbital Angular Momentum of a Single Photon. *Phys. Rev. Lett.* **2002**, *88*, 257901. [[CrossRef](#)]
10. Kapale, K.T.; Dowling, J.P. Vortex Phase Qubit: Generating Arbitrary, Counterrotating, Coherent Superpositions in Bose-Einstein Condensates via Optical Angular Momentum Beams. *Phys. Rev. Lett.* **2005**, *95*, 173601. [[CrossRef](#)]
11. Zeng, J.; Liang, C.; Wang, H.; Wang, F.; Zhao, C.; Gbur, G.; Cai, Y. Partially Coherent Radially Polarized Fractional Vortex Beam. *Opt. Express* **2020**, *28*, 11493–11513. [[CrossRef](#)] [[PubMed](#)]
12. Tao, S.H.; Yuan, X.-C.; Lin, J.; Peng, X.; Niu, H.B. Fractional Optical Vortex Beam Induced Rotation of Particles. *Opt. Express OE* **2005**, *13*, 7726–7731. [[CrossRef](#)] [[PubMed](#)]
13. Toyoda, K.; Miyamoto, K.; Aoki, N.; Morita, R.; Omatsu, T. Using Optical Vortex to Control the Chirality of Twisted Metal Nanostructures. *Nano Lett.* **2012**, *12*, 3645–3649. [[CrossRef](#)] [[PubMed](#)]
14. Shelby, R.A.; Smith, D.R.; Schultz, S. Experimental Verification of a Negative Index of Refraction. *Science* **2001**, *292*, 77–79. [[CrossRef](#)] [[PubMed](#)]
15. Dholakia, K.; Simpson, N.B.; Padgett, M.J.; Allen, L. Second-Harmonic Generation and the Orbital Angular Momentum of Light. *Phys. Rev. A* **1996**, *54*, R3742–R3745. [[CrossRef](#)] [[PubMed](#)]
16. Li, Y.; Zhou, Z.-Y.; Ding, D.-S.; Shi, B.-S. Sum Frequency Generation with Two Orbital Angular Momentum Carrying Laser Beams. *J. Opt. Soc. Am. B* **2015**, *32*, 407–411. [[CrossRef](#)]
17. Rao, A.S.; Miyamoto, K.; Omatsu, T. Direct Generation of Vortex Lattice Modes from an Intracavity Frequency Doubled Pr:YLF Laser. In Proceedings of the Conference on Lasers and Electro-Optics, San Jose, CA, USA, 9–14 May 2021. p. STh1B.2. [[CrossRef](#)]
18. Niu, S.; Wang, S.; Ababaik, M.; Yusufu, T.; Miyamoto, K.; Omatsu, T. Tunable Near- and Mid-Infrared (1.36–1.63 Mm and 3.07–4.81 Mm) Optical Vortex Laser Source. *Laser Phys. Lett.* **2020**, *17*, 045402. [[CrossRef](#)]
19. Zhu, H.; Guo, J.; Duan, Y.; Zhang, J.; Zhang, Y.; Xu, C.; Wang, H.; Fan, D. Efficient 1.7 Mm Light Source Based on KTA-OPO Derived by Nd:YVO₄ Self-Raman Laser. *Opt. Lett.* **2018**, *43*, 345–348. [[CrossRef](#)] [[PubMed](#)]
20. Abulikemu, A.; Yakufu, S.; Zhou, Y.X.; Yusufu, T. Mid-Infrared Idler-Resonant Optical Vortex Parametric Oscillator Based on MgO:PPLN. *Opt. Laser Technol.* **2024**, *171*, 110341. [[CrossRef](#)]
21. Zhou, Y.; Yusufu, T.; Ma, Y.; Omatsu, T. Generation of Tunable, Non-Integer OAM States from an Optical Parametric Oscillator. *Appl. Phys. Lett.* **2023**, *122*, 121106. [[CrossRef](#)]
22. Liu, J.; Duan, Y.; Li, Z.; Zhang, G.; Zhu, H. Recent Progress in Nonlinear Frequency Conversion of Optical Vortex Lasers. *Front. Phys.* **2022**, *10*, 865029. [[CrossRef](#)]
23. Baumgartner, R.; Byer, R. Optical Parametric Amplification. *IEEE J. Quantum Electron.* **1979**, *15*, 432–444. [[CrossRef](#)]
24. Lee, A.J.; Omatsu, T.; Pask, H.M. Direct Generation of a First-Stokes Vortex Laser Beam from a Self-Raman Laser. *Opt. Express* **2013**, *21*, 12401–12409. [[CrossRef](#)] [[PubMed](#)]
25. Hu, L.; Ning, J.; Chen, Y.; Lv, X.; Zhao, G.; Xu, P.; Zhu, S. Continuous-Wave Operation of a Tandem Optical Parametric Oscillator up to 5.19 Mm Based on Periodically Poled LiNbO₃. *Opt. Lett.* **2024**, *49*, 931–934. [[CrossRef](#)] [[PubMed](#)]
26. Ababaik, M.; Wang, S.; Aierken, P.; Omatsu, T.; Yusufu, T. Near and Mid-Infrared Optical Vortex Parametric Oscillator Based on KTA. *Sci. Rep.* **2021**, *11*, 8013. [[CrossRef](#)] [[PubMed](#)]
27. Rao, A.S.; Yadav, D.; Samanta, G.K. Nonlinear Frequency Conversion of 3D Optical Bottle Beams Generated Using a Single Axicon. *Opt. Lett.* **2021**, *46*, 657–660. [[CrossRef](#)] [[PubMed](#)]
28. Yang, Y.; Li, Y.; Wang, C. Generation and Expansion of Laguerre–Gaussian Beams. *J. Opt.* **2022**, *51*, 910–926. [[CrossRef](#)]
29. Fang, X.; Yang, G.; Wei, D.; Ni, R.; Ji, W.; Zhang, Y.; Hu, X.; Hu, W.; Lu, Y.Q.; et al. Coupled Orbital Angular Momentum Conversions in a Quasi-Periodically Poled LiTaO₃ Crystal. *Opt. Lett.* **2016**, *41*, 1169–1172. [[CrossRef](#)] [[PubMed](#)]
30. Wang, J.; Yang, J.-Y.; Fazal, I.M.; Ahmed, N.; Yan, Y.; Huang, H.; Ren, Y.; Yue, Y.; Dolinar, S.; Tur, M.; et al. Terabit Free-Space Data Transmission Employing Orbital Angular Momentum Multiplexing. *Nat. Photon.* **2012**, *6*, 488–496. [[CrossRef](#)]
31. Fang, X.; Yang, H.; Yao, W.; Wang, T.; Zhang, Y.; Gu, M.; Xiao, M. High-Dimensional Orbital Angular Momentum Multiplexing Nonlinear Holography. *Adv. Photon.* **2021**, *3*, 015001. [[CrossRef](#)]
32. Agrell, E.; Karlsson, M.; Chraplyvy, A.R.; Richardson, D.J.; Krummrich, P.M.; Winzer, P.; Roberts, K.; Fischer, J.K.; Savory, S.J.; Eggleton, B.J.; et al. Roadmap of Optical Communications. *J. Opt.* **2016**, *18*, 063002. [[CrossRef](#)]

33. Ren, H.; Li, X.; Zhang, Q.; Gu, M. On-Chip Noninterference Angular Momentum Multiplexing of Broadband Light. *Science* **2016**, *352*, 805–809. [[CrossRef](#)] [[PubMed](#)]
34. Ebrahim-Zadeh, M.; Sorokina, I.T. (Eds.) *Mid-Infrared Coherent Sources and Applications*; Springer Science & Business Media: Berlin/Heidelberg, Germany, 2008.
35. Li, S.-M.; Kong, L.-J.; Ren, Z.-C.; Li, Y.; Tu, C.; Wang, H.-T. Managing Orbital Angular Momentum in Second-Harmonic Generation. *Phys. Rev. A* **2013**, *88*, 035801. [[CrossRef](#)]
36. Patton, B.R.; Burke, D.; Oswald, D.; Gould, T.J.; Bewersdorf, J.; Booth, M.J. Three-Dimensional STED Microscopy of Aberrating Tissue Using Dual Adaptive Optics. *Opt. Express* **2016**, *24*, 8862–8876. [[CrossRef](#)] [[PubMed](#)]
37. Toyoda, K.; Takahashi, F.; Takizawa, S.; Tokizane, Y.; Miyamoto, K.; Morita, R.; Omatsu, T. Transfer of Light Helicity to Nanostructures. *Phys. Rev. Lett.* **2013**, *110*, 143603. [[CrossRef](#)] [[PubMed](#)]
38. Takahashi, F.; Miyamoto, K.; Hidai, H.; Yamane, K.; Morita, R.; Omatsu, T. Picosecond Optical Vortex Pulse Illumination Forms a Monocrystalline Silicon Needle. *Sci. Rep.* **2016**, *6*, 21738. [[CrossRef](#)] [[PubMed](#)]
39. Sharma, V.; Kumar, S.C.; Samanta, G.K.; Ebrahim-Zadeh, M. Orbital Angular Momentum Exchange in a Picosecond Optical Parametric Oscillator. *Opt. Lett.* **2018**, *43*, 3606–3609. [[CrossRef](#)] [[PubMed](#)]
40. Sharma, V.; Kumar, S.C.; Samanta, G.K.; Ebrahim-Zadeh, M. Multi-Structured-Beam Optical Parametric Oscillator. *Opt. Express* **2020**, *28*, 21650–21658. [[CrossRef](#)] [[PubMed](#)]
41. Sharma, V.; Kumar, S.C.; Samanta, G.K.; Ebrahim-Zadeh, M. Tunable Vortex Beam Generation Using an Optical Parametric Oscillator with an Antiresonant-Ring Interferometer. *Opt. Lett.* **2021**, *46*, 3235–3238. [[CrossRef](#)]
42. Sharma, V.; Kumar, S.C.; Samanta, G.K.; Ebrahim-Zadeh, M. Tunable, High-Power, High-Order Optical Vortex Beam Generation in the Mid-Infrared. *Opt. Express* **2022**, *30*, 1195–1204. [[CrossRef](#)]
43. Jashaner, D.; Zhou, Y.; Yusufu, T. Widely-Tunable Mid-Infrared (2.6–5 μm) Picosecond Vortex Laser. *Appl. Phys. Express* **2022**, *15*, 102004. [[CrossRef](#)]
44. Vaity, P.; Banerji, J.; Singh, R.P. Measuring the Topological Charge of an Optical Vortex by Using a Tilted Convex Lens. *Phys. Lett. A* **2013**, *377*, 1154–1156. [[CrossRef](#)]
45. Zavadilová, A.; Kubeček, V.; Diels, J.-C.; Šulc, J. Dual Pulse Operation of 1.5 μm Picosecond Intracavity Synchronously Pumped Optical Parametric Oscillator. In Proceedings of the 7th International Conference on Photonics, Devices, and Systems V, Prague, Czech Republic, 24–26 August 2011; SPIE: Bellingham, WA, USA, 2011; Volume 8306, pp. 317–322.

Disclaimer/Publisher's Note: The statements, opinions and data contained in all publications are solely those of the individual author(s) and contributor(s) and not of MDPI and/or the editor(s). MDPI and/or the editor(s) disclaim responsibility for any injury to people or property resulting from any ideas, methods, instructions or products referred to in the content.